Supporting information

Highly-robust solid oxide fuel cell (SOFC): simultaneous greenhouse gas treatment and clean energy generation

T. Li, M. Rabuni, L. Kleiminger, B. Wang, G.H. Kelsall, U.W. Hartley and K. Li*

Experimental

Materials: Yttria-stabilized zirconia (YSZ8), Lanthanum strontium manganite ($La_{0.8}Sr_{0.2}MnO_{3-\delta}$) and nickel oxide (NiO) were purchased from Inframat Advanced Materials (USA). Polyethersulfone (PESf) (Radal A300, Ameco Performance, USA), 30-dipolyhydroxystearate (Arlacel P135, Uniqema), dimethyl sulfoxide (DMSO, HPLC grade, VWR) and ethanol (HPLC grade, VWR) were used as the polymer binder, dispersant and solvent, respectively. Polyvinyl alcohol (PVA, M.W. approx. 145000, Merck Schuchardt OHG, Germany) was used as internal coagulant.

Fuel Cell Fabrication: The 3-channel anode support was fabricated via a phase inversion-assisted process, which is similar conventional hollow fiber fabrication as described elsewhere [1]. Generally, a suspension composed of ceramic particles, solvent and polymer binder was mixed for 3-4 days via planetary ball milling (SFM-1 Desk-top Miller, MTI Corporation, USA) to obtain proper homogeneity. The miller was operated at 263 rpm with 40 yttria-stabilized zirconia (YSZ3) milling balls (10 mm diameter) and 200 g of powder in each milling jar. Details of the suspension composition could be found in Table S1. Prior to being transferred into stainless steel syringes, the suspension was degassed under vacuum to fully eliminate air bubbles trapped inside. The whole spinning procedure is controlled by syringe pumps (Harvard PHD22/200 HPsi) to achieve precise control over extrusion rates of various components. It's noteworthy that the internal coagulant, which is 10 wt.% PVA aqueous solution, is split into required number of streams by a custom-designed nozzle before in contact with suspension to form the multi-channel structure. The precursor fibers were removed from the external coagulant bath after the phase-inversion is completed, and then dried and straightened at room temperature. Details of the triple-nozzle design are depicted in Figure S1 and triple-nozzle component could be easily changed to the other

components with different nozzle numbers. YSZ electrolyte was prepared by dip-coating process and detailed composition of the coating ink is shown in Table S1. Anode precursors were dipped into ink and pulled up with a withdraw speed of 2 mm s^{-1}. After the coated electrolyte was dried, the anode and electrolyte were co-sintered at 1450 °C for 6 hours. Finally the dual-layer cathode was dip-coated onto the sintered half-cell. After both layers were dried, a sintering process at 1100 °C was undertaken for 3 hours. The thickness of each cathode layer is approximately 15 µm.

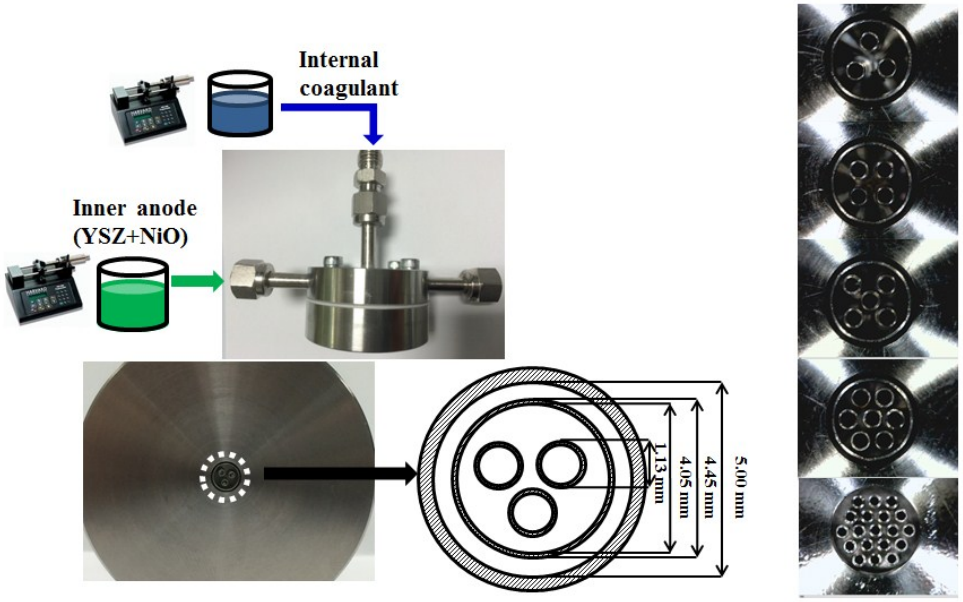

Figure S1 Schematic diagram of extrusion process and dimensions of multi-nozzle spinneret.

Table S1. Compositions of anode suspension and electrolyte coating ink.

Component	Composition (wt.%)				
Anode	YSZ	NiO	DMSO	PESf	Arlancel P135
	24.4	36.7	30.6	7.6	0.6
Electrolyte	YSZ	Ethanol	PVB	PEG	Arlancel P135
	28.2	67.8	1.8	1.0	1.1

Gas-tightness test: The gas-tightness property of electrolyte was investigated using a N_2 permeation method described elsewhere [2]. A pressure gauge was adopted to monitor the

pressure change of the permeation set-up. The N_2 permeability was calculated based on the pressure change over a certain length of time (5 hours).

$$P = \frac{V}{RT \times A_m t} \ln\left(\frac{p_0 - p_a}{p_t - p_a}\right) \quad \text{(S1)}$$

Where P denotes the permeability of the test membrane (mol $m^{-2}s^{-2}Pa^{-1}$); V is the volume of the test vessel (m^3); R is the gas constant (8.314 J $mol^{-1}K^{-1}$); T denotes the measured temperature (K); p_0, p_a, p_t represent the initial, atmospheric and final pressure readings (Pa), respectively. A_m is the membrane area (m^2), which is calculated by $A_m = \left[2\pi(R_o - R_{in})L\right] / \ln(R_o / R_{in})$, where R_o and R_{in} denote the outer and inner radiuses of the hollow fiber, respectively; L is the length of the fiber and t is the time for the measurement (s).

Mechanical strength test: The mechanical strength of the hollow fibers was measured by a tensile tester (Instron Model 5544) with a load cell of 1 kN. This measurement was conducted via a three-point bending method. Fiber samples were positioned onto a sample holder with a distance of 30 mm [3].

Electrochemical characterization: Silver wires of 0.2 mm diameter (99.99% purity, Advent Materials Ltd, UK) were wrapped along cathode and on exposed anode for current collection. Silver paste was painted to improve the contact between wires and electrode surface. The completed single cell was fixed into two gas-tight alumina tubes (Multi-lab Ltd, UK) and sealed with ceramic sealant (Aremco, Ceramabond 552-VFG). Wires from both electrodes were connected to a potentiostat/galvanostat (Iviumstat, Netherlands) for subsequent electrochemical performance tests, as illustrated in Figure S2. These measurements were conducted between 650-750 °C, with 30 ml min^{-1} of pure H_2 fed to anode as the fuel and 50 ml min^{-1} of oxidant (air, N_2O or pure O_2) fed to cathode as oxidant. Electrochemical impedance spectroscopy (EIS) analysis was undertaken under open-circuit conditions in the frequency range of 10^5-0.01 Hz with signal amplitude of 10 mV.

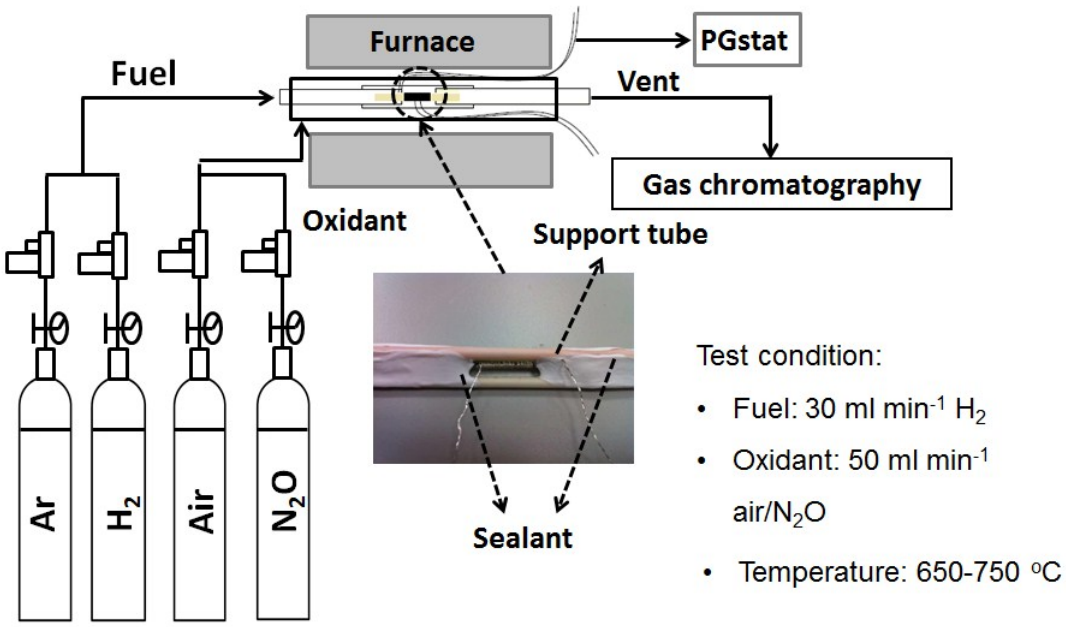

Figure S2 Experimental set-up of electrochemical characterizations and test conditions.

N_2O conversion: The analysis of shell-side effluent was performed on-line by gas chromatography (Varian 3900) with thermal conductivity detector (TCD). The N_2O conversion was calculated using the equation: (N_2O conversion) = (% N_2 by GC) / [(% N_2 by GC)+(% N_2O by GC)].

The calibration curves for N2O and gas composition results are shown in Figure S3 and Table S2, respectively.

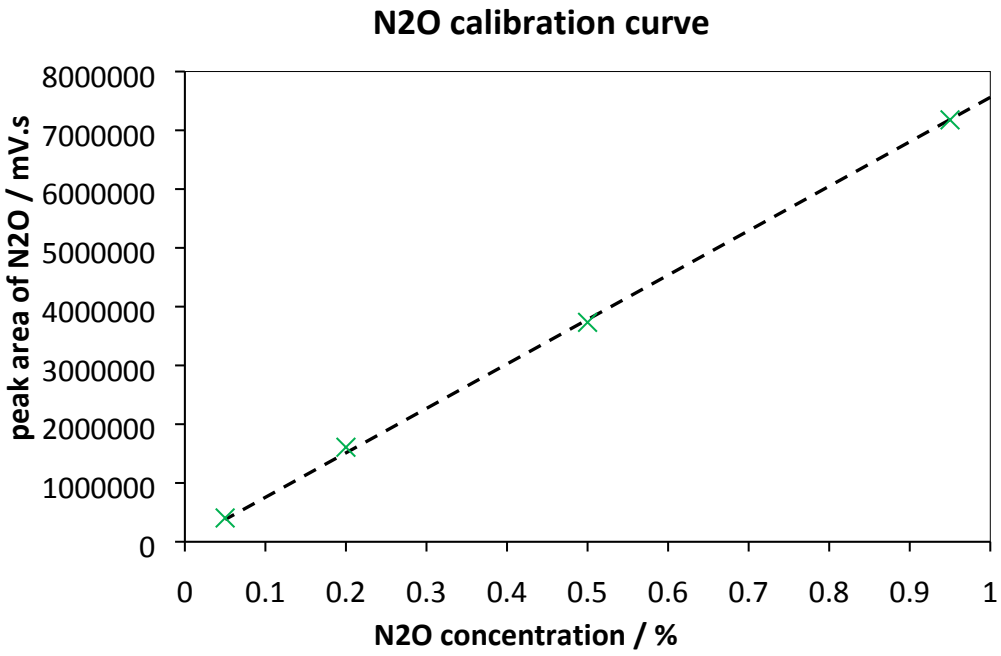

Figure S3. Calibration curve of gas chromatography of N_2O (argon as carrier gas)

Table S2: Percentage of the gases measured by gas chromatography using argon as sweep gas [a].

T/°C	% N_2 by GC[b]	Ave. peak area for N_2O (mV.s, ±0.5%)	% N_2O by GC	N_2O conversion (%)
650	22.3	4321377	57.1	28.1
700	32.5	3096492	40.9	44.3
750	38.2	2307796	30.5	55.6

[a] % N_2 was calculated using the N_2 calibration equation: (% N_2) = (peak area of N_2+19809.7)/113479267. The remaining of gas in the mixture is oxygen.

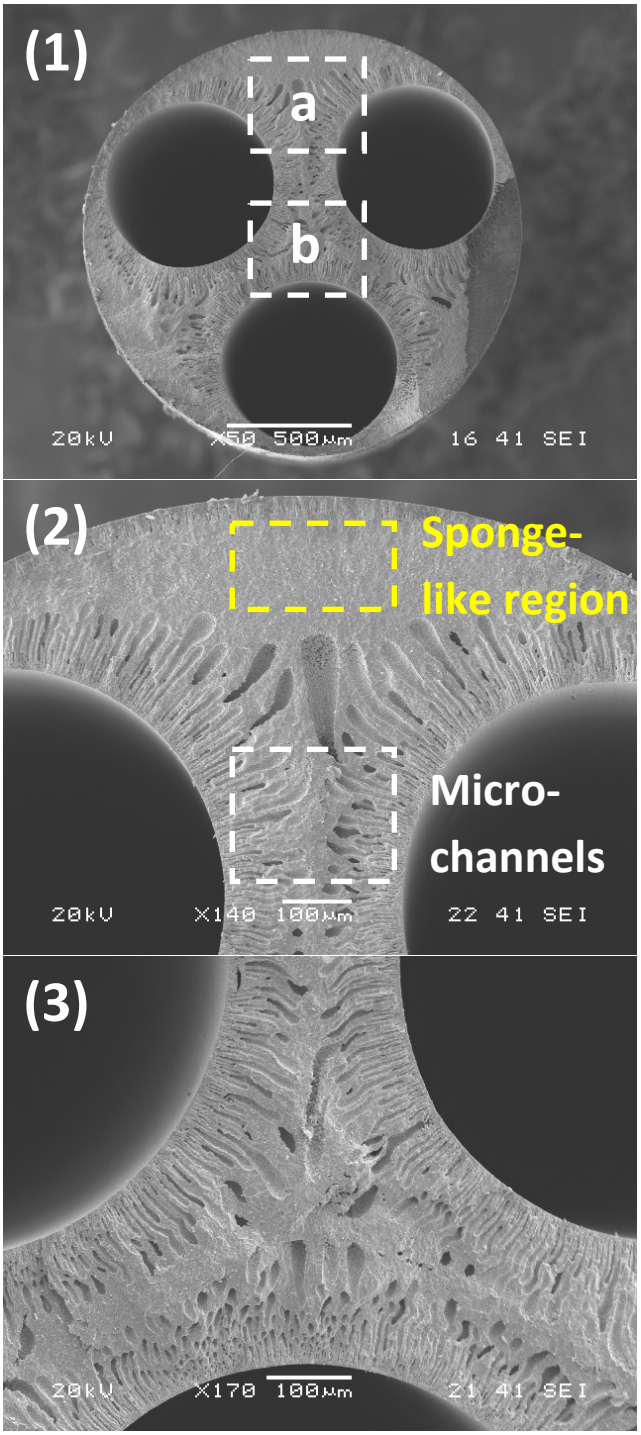

Figure S4. (1) overview of cross-section of 3-channel micro-tube; (2) magnified view of Zone (a) in Figure S4 (1); (3) magnified view of Zone (b) in Figure S4 (1).

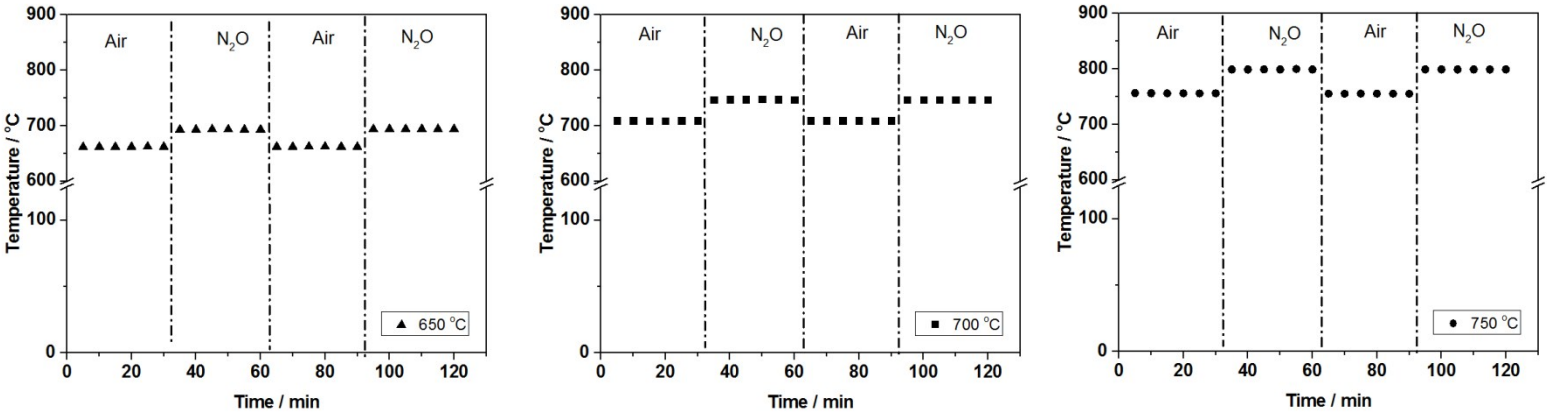

Figure S5. Temperature change near LSM during air-N_2O cycling (each atmosphere was dwelled for 30 min).

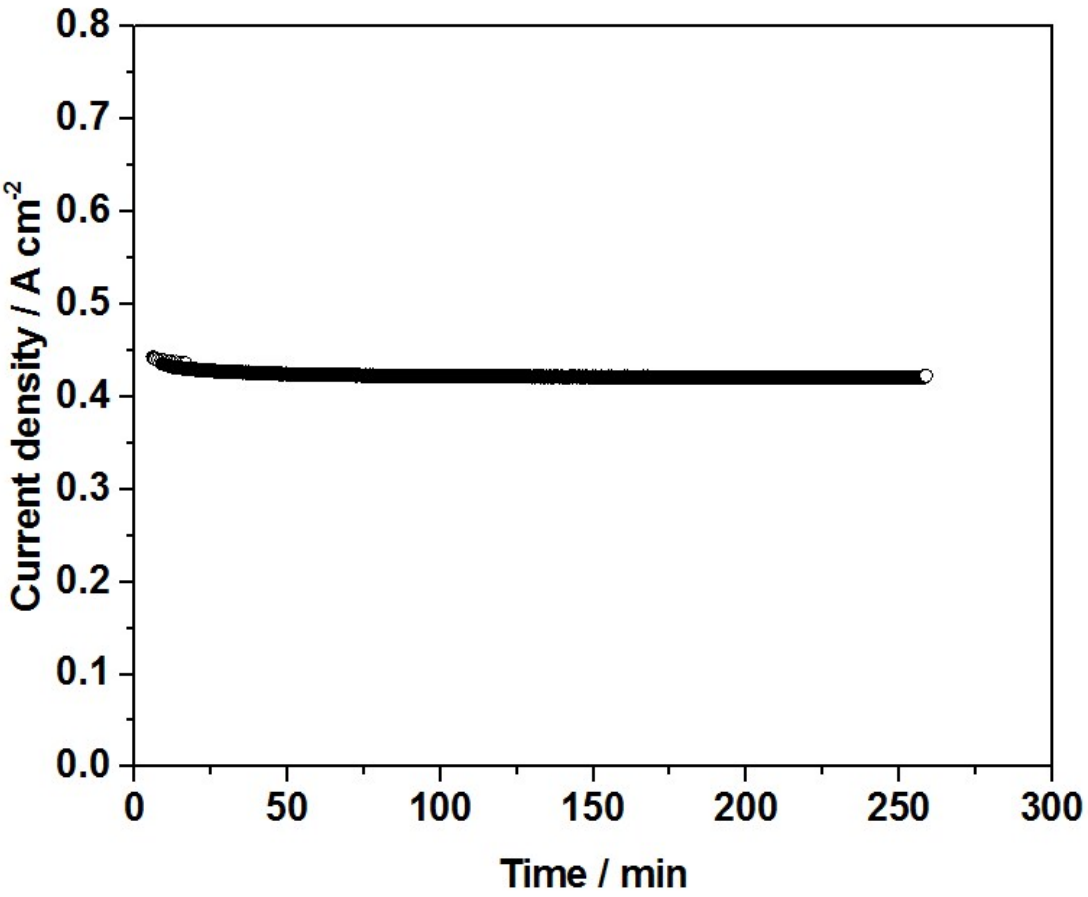

Figure S6. Stability test conducted at 0.7V, 750 °C. (50 ml min^{-1} N_2O as oxidant and 30 ml min^{-1} H_2 as the fuel)

Techno-economic evaluation

Outline: To achieve a profitable process, one should first determine the electricity sales price, at which the revenue generated by the electricity sales will exceed the costs of running the plant. These costs are comprised of fixed costs, which includes the capital expenditure of fuel cell stack and auxiliary equipment as well as the maintenance and the variable costs, which include the fuel feed costs, heating and electrical energy inputs. The steps of the techno-economic analysis include:

- Plant overview (set plant scope, operating conditions, assumptions and reactant/product flow rate calculations)
- Capital equipment sizing
- Capital equipment costing
- Determine operating expenditure

Plant overview: The main anthropogenic N_2O emission is produced during nitric acid production. In the USA are 41 nitric acid production plants (as of 2010), emitting 61×10^4 metric tonnes of N_2O annually (based on 19 million metric tonnes of CO_2 equivalent and a global warming potential of 310 for N_2O), corresponding to ca. 1500 metric tonnes of N_2O per plant per annum. [4]

Figure S6 shows the proposed plant layout for using N_2O as the oxidant in a solid oxide fuel cell (SOFC) operating on methane (without reforming [5]). Plant specifications, operating conditions and assumptions are outlined in Table S3. The resulting stream table using feed values and pre-set conversions is summarised in Table S4.

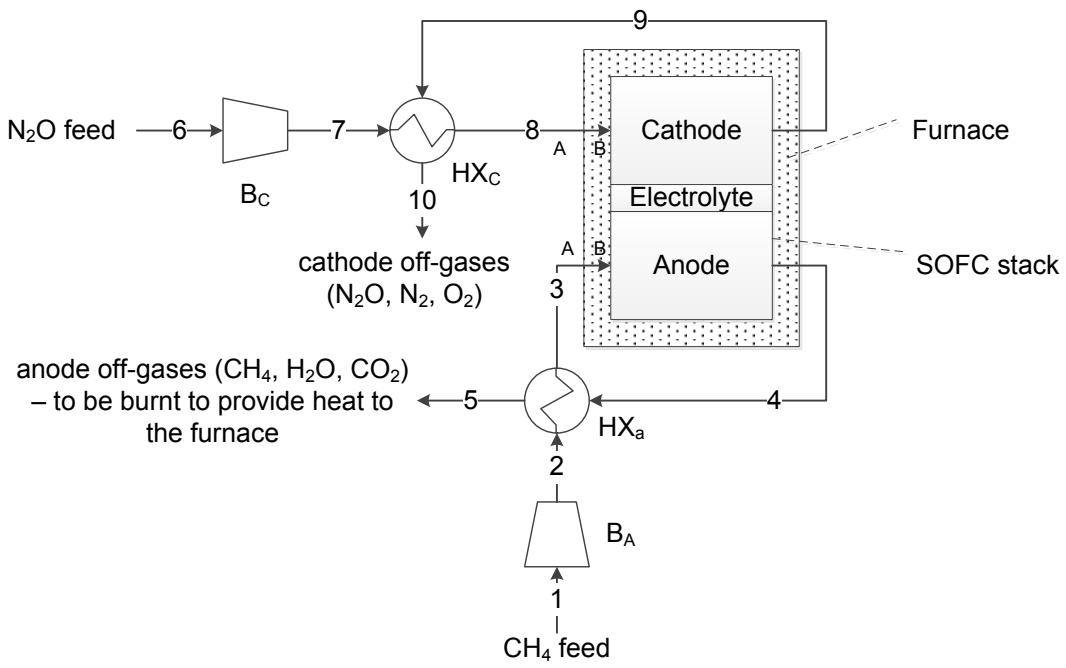

Figure S7. Plant layout for solid oxide fuel cell operating on CH_4 and N_2O, with HX = heat exchanger and B = blower.

Table S3: Plant Specifications for 0.2 tonne of N_2O treated per hour

Operating conditions	Values	Reference and comments
Temperature	750 °C	
Cell potential difference	0.5 V	Peak-power density (0.3 W cm^{-2})
Current density	0.6 A cm^{-2}	Peak-power density (0.3 W cm^{-2})
N_2O conversion	95 %	
Oxygen utilisation	50%	
Utilisation of CH_4	70%	Unreacted off-gases are burnt to pre-heat the gases and maintain the temperature within the furnace.
Reactant gases supply temperatures	25 °C	Gases are pre-heated before the SOFC stack using heat exchangers and furnace.
Pressure	0.1 MPa	
Plant life time	20 years	With a SOFC stack life of 5 years [6], operating for 7500 hours a year.

Table S4: Stream table for plant design outlined in Figure S6.

	Anode side						Cathode side					
	1	2	3A	3B	4	5	6	7	8A	8B	9	10
N_2O molar flow rate / mol hr^{-1}							4545	4545	4545	4545	227	227
N_2 molar flow rate / mol hr^{-1}											4318	4318
O_2 molar flow rate / mol hr^{-1}											1080	1080
CH_4 molar flow rate / mol hr^{-1}	771	771	771	771	231	231						
H_2O molar flow rate / mol hr^{-1}					1080	1080						
CO_2 molar flow rate / mol hr^{-1}					540	540						
Temperature[1] / °C	25.0	38.7	720	750	750	295	25.0	38.7	495	750	750	68.7

[1] The blower outlet temperature, was calculated using: $T_{outlet} = \frac{T_{inlet}}{\eta_{isothermal\ efficiency}}\left(R^{0.286} - 1\right) + T_{inlet}$ with compression ratio: R= 1.1 and isothermal efficiency: η= 0.6. [7]

Capital equipment sizing: The fuel cell stack was sized based on its 'reacted' CH_4 molar throughput of 540 mol hr^{-1} resulting in a required reactor area of 19.3 m^2 using equation (S2), where *F* is the Faraday's constant (96485 s A mol^{-1}), *dn/dt* the molar flow rates and *j* the current density of the cell.

$$A_{reactor} / m^2 = 8F \frac{dn}{dt} \times \frac{1}{j} \quad \text{(S2)}$$

The blowers (B_A and B_C, where A and C denote the anode and cathode side, respectively) were sized according to their volumetric flow rates.

For the counter-current heat exchangers a minimum temperature difference between hot and cold streams of 30 °C was set. The available/required heat duties (*Q*) and resulting temperatures for the hot/cold stream were determined from (S3) with the efficiency (η) set at 0.9, where C_p is the molar heat capacity [8] of an individual stream component (i), *T* denotes temperature and $\dot{n}$ is the molar flow rate.

$$|Q| / kW = \sum_i C_{p,i} \times \left| \left(T_{final} - T_{intial} \right) \right| \times \dot{n}_i \times \eta \quad \text{(S3)}$$

The required heat exchanger areas were determined from (S4) with the overall heat transfer coefficient (*U*) set at 30 W $°C^{-1}$ m^{-2} for gas-gas transfer [9] and a log mean temperature difference calculated according to (S5).

$$Area_{heat\ exchanger} / m^2 = \frac{Q}{U \Delta T_{lm}} \quad \text{(S4)}$$

$$\Delta T_{lm} = \frac{\left(T_{h,in} - T_{c,out} \right) - \left(T_{h,out} - T_{c,in} \right)}{\ln \left(\frac{T_{h,in} - T_{c,out}}{T_{h,out} - T_{c,in}} \right)} \quad \text{(S5)}$$

Using equation S4 the remaining* heat duty to raise the temperature of the reactant gas stream to the operating temperature was calculated using a furnace efficiency of 0.9.

Capital equipment costing: The purchase cost of individual industrially available equipment (*i.e.* blowers, heat exchangers and furnace) was determined using cost correlations [9, 10].

For the SOFC stack, the production cost were estimated as twice the material cost. First, for

* Note: the initial start-up and shut-down operational requirements have not been addressed in the sizing calculations.

an individual fiber, the mass of yttria-stabilised zirconia (YSZ), nickel oxide and lanthanum strontium manganite (LSM) was calculated based on the dimensions in Figure 2 with a total fiber length of 50 mm and a 10 mm long LSM-YSZ|LSM electrode (0.56 cm^2 active electrode area). Porosities of 0.15, 0.2 and 0.2 for the NiO-YSZ (prior to reduction), LSM-YSZ and LSM were assumed, respectively [11]. Current collection using 2 × 0.1 m long silver wires (0.2 mm diameter) for each fiber was proposed.[†]

For 1 m^{-2} of active area ca. 18175 fibers were required. Using raw material prices of $ 71.6 kg^{-1}, $ 290 kg^{-1}, $ 74 kg^{-1} and $ 0.245 m^{-1} for YSZ, LSM, NiO and silver wire respectively [11], the costs for SOFC stack manufacture were estimated to be *ca.* $ 2900 m^{-2}.

Capital investment for installed units was estimated using Hand Factors (multiplying factor to be applied to the individual purchase costs), which have been reported as 2.5, 3.5, 2.5 and 2.0 for electrolyser, heat exchangers, blowers and furnaces, respectively [9]. Replacement costs of SOFC stacks (every 5 years) were taken as purchased equipment costs only.

Thus, operating for 7500 years over 20 years, the capital expenditure (CAPEX) per tonne of N_2O was *ca.* $ 11.9. 71% of the CAPEX were associated with the SOFC stack.

Determining operating expenditure (OPEX): Maintenance was set at 10% of the CAPEX [6]; hence, $ 1.19 per tonne of N_2O. Blower and furnace energies were based on the difference in specific heat of the streams per hour. The electrical energy for the blower was deducted from the fuel cell power output; whereas the energy required to heat the furnace was provided by the unreacted fuel side (anode) off-gases (heating value [12] of methane was 13.9 kWh kg^{-1}). The natural gas price in the US (May 2016) was $ 2.91 per 1000 ft^3 equivalent to *ca.* $ 0.16 kg^{-1} [13].

[†] This is an overestimate for commercial SOFC stacks. The proposed silver current collection would contribute 61% towards the total cost compared to 39% for functional metal oxides. However, this allows to reflect uncertainties in the stack design costs.

References

[1] T. Li, Z. Wu, K. Li, Journal of Membrane Science, 449 (2014) 1-8.
[2] Xiaoyao Tan, Yutie Liu, K. Li, AIChE Journal, 51 (2005) 1991-2000.
[3] S. Liu, Ceramics International, 29 (2003) 875-881.
[4] EPA, 'Available and emerging technologies for reducing greenhouse gas emissions from the nitric acid production industry', United States Environmental Protection Agency, 2010, USA.
[5] S. Park, J.M. Vohs, R.J. Gorte, Nature, 404 (2000) 265-267.
[6] C. Graves, S.D. Ebbesen, M. Mogensen, K.S. Lackner, Renew. Sust. Energ. Rev., 15 (2011) 1-23.
[7] J. Larminie and A. Dicks, 'Fuel Cell Systems Explained, 2nd Edition ed., Chichester, UK, John Wiley & Sons, 2003, pp. 309-330.
[8] M.W. Chase, NIST-JANAF Thermochemical Tables, 4th Edition, J. Phys. Chem. Ref. Data, Monograph 9 (1998) 1-1951.
[9] R. Sinnott and G. Towler, Chemical Engineering Design, 5th Edition, Oxford, UK, Butterworth-Heinemann, 2009.
[10] Matches, 'Matches' Process Equipment Cost Estimates',
http://www.matche.com/equipcost/Default.html , 2014 (accessed 12/08/2016).
[11] L. Kleiminger, 'Solid oxide electrochemical reactors and processes for CO_2 and H_2O splitting', Ph.D Thesis, Imperial College London, UK, 2015.
[12] P.P. Edwards, V.L. Kuznetsov, W.IF. David, N.P. Brandon, Energy Policy, 36 (2008) 4356-4362.
[13] U.S. Energy Information Administration (EIA), 'United States Natural Gas Industrial Price', https://www.eia.gov/dnav/ng/hist/n3035us3m.htm, 2016 (accessed 12/08/2016).